Oxid Met (2015) 84:151–167
DOI 10.1007/s11085-015-9548-1

ORIGINAL PAPER

Phase Transformations in Pt-Aluminide Coatings and Their Effect on Oxidation Resistance

C. Fu[1,2] · S. Q. Wang[1,2] · W. K. Kong[1,2] · G. H. Cao[1,2]

Received: 27 January 2015 / Revised: 26 February 2015 / Published online: 5 April 2015

Abstract Diffusion coatings have been widely used as metallic bond coatings in thermal barrier systems to protect aeronautical turbine blades from detrimental oxidation and hot corrosion. A cooling scheme is one of most effective methods to protect a material surface exposed to a high temperature environment. However, fast cooling rate will not only generate thermal damages by high thermal stresses, but also affect the structure of coatings. An experimental program was undertaken to study the effects of cooling rates on the microstructure of Pt-aluminide coatings after diffusion treatment at high temperatures followed by furnace-cooling and water-quenching treatments. In order to further study the effects of the phase transformation on coatings, the Al-deposited coatings were prepared by the pack cementation process to increase the Al content in Pt-aluminide coatings and the microstructures of these coatings were also investigated. The composition (in wt%) of the packs was xAl-2NH_4Cl-(98 − x)Al_2O_3 with different Al levels (x = 1, 4 and 6) and the Pt-aluminide coatings were transformed to ε-PtAl, ξ-$PtAl_2$ or γ′-(Ni, Pt)$_3$Al after Al deposition. Isothermal oxidation tests were performed in air at 1000 °C for up to 100 h. These oxidation tests indicated that parabolic scaling kinetics were established and that the coating formed in the packs containing 1 wt% Al exhibited slower scale growth rate. After oxidation, the oxidation scales, Al_2O_3 or Cr_2O_3, were formed above the coatings. The mechanisms of phase transformations in Pt-aluminide coatings after furnace-cooling and water-quenching treatments

✉ G. H. Cao
ghcao@shu.edu.cn

[1] Department of Materials Engineering, Shanghai University, 149 Yanchang Road, Shanghai 200072, China

[2] State Key Laboratory of Advanced Special Steel, Shanghai University, 149 Yanchang Road, Shanghai 200072, China

are discussed. In addition, the effects of these phase transformations on the oxidation resistance of the coatings are also discussed.

Keywords Thermal barrier coatings · Water quenching · Microstructure · Oxidation · α-NiPt

Introduction

The demand for improved performance in high-temperature mechanical systems has led to increasingly harsh operating environments, particularly for the components in advanced gas turbine engines. In order to enhance the thermal efficiency of gas turbine, rocket, and ramjet systems, the operating temperature of aero-engine become much higher [1], which is above the melting point of Ni-based superalloys. To protect these thermal power systems, various cooling methods have been used. A typical cooling system with both the structural materials such as thermal barrier coatings (TBCs) and film cooling scheme is critically important to the performance and safety of aeroengine turbines [2, 3]. Nowadays, TBCs are still the most widely used commercial materials because of their excellent performances that can bear the influences of suddenly changes in temperature, thermal stress, or corrosion gas. TBCs durability is related to the design of the cooling systems. Current state-of-the-art bond coatings for TBCs systems are either β-(Ni, Pt)Al or MCrAlY (M = Ni, Co or Ni + Co), both of which possess high aluminum content. These coatings are highly effective in protecting the components against high-temperature oxidation due to their ability to form a dense and slow thermally grown oxide (TGO) Al_2O_3 scale that acts as a diffusion barrier, substantially reducing the rate of oxidation [4–6]. However, the aluminum depletion degrades the bond coating by surface deformation/rumpling, martensitic transformation together with volume change and crack [7–9].

Recently, Gleeson et al. [10] reported that a wide range of Pt-modified γ-Ni + γ′-Ni_3Al alloy compositions could form a slow-growing Al_2O_3 scale. These alloys can be used as an alternative coating for the current β-based coatings [11]. The γ′-Ni_3Al intermetallic compound is of great importance due to its excellent high-temperature strength as well as its high-temperature oxidation resistance [12]. Compared with the β-(Ni, Pt)Al or MCrAlY coatings, the Pt-modified γ-Ni + γ′-Ni_3Al coatings are more compatible with the high-temperature alloys and are able to form a more planar Al_2O_3 scale, which is very important for a reliable TBCs system [13].

To combat and avert the blade failure caused by high operating temperature, film cooling has been widely used in the aeroengine. It is well known that the wall temperature in a film cooling system is changed dynamically by flow mixing of the hot gas and cooling air [3]. The thermal stress caused by thermal cycles will be generated and be detrimental for the reliability of TBCs. The coating systems usually undergo thermal cycles during use and the microstructure of the coatings would be changed caused by fast cooling rate. Therefore, it is important to deeply understand the relationship between microstructure of coatings and cooling rate. However, current studies about the Pt-Aluminide coatings prepared by different

cooling rates are lacked, which is of importance for high-temperature mechanical systems, as this may have obvious effects on the microstructure and performance. Many precious studies focus on thermal stress and damages caused by large thermal gradients, which are common in the aeroengine systems and can cause residual stresses, distortion, thermal cracks, structural failure or changes in the microstructure. These damages are undesirable because they can potentially accelerate coating spallation under cyclic heating and cooling during operation. Sundaram et al. have illustrated that stresses and strain energy generated by thermal transients can cause failure in the TBCs, and they also pointed out that the cooling rate is related to the variation in the thickness, modulus, and thermal expansion of the coatings [14]. The stresses generated by the quasi-steady state temperature by slow cooling can be deleterious to TBCs and differential cooling of the coating as compared to the substrate creates additional stresses that promote delamination [15]. Failure occurs during thermal cycles because thermal mismatch between the TGO scale and TBCs generates high stresses caused by cooling during hot time of the aeroengine system [16].

Although the film cooling among the recent cooling methods has been widely used, the study on the microstructure and performance of coatings due to cooling rate has not been investigated. In this study, we synthesized the Pt-Aluminide coatings by water-quenching and furnace-cooling treatments and studied the effects of cooling rate on microstructure, distribution of Al and Cr, and oxidation performance of coatings. The aim of the research is to pinpoint the phase transformations in Pt-Aluminide coatings prepared by diffusion treatment at high temperatures followed by cooling treatments in different cooling rates. The effects of these phase transformations on the distribution of Cr and oxidation resistance of coatings are also discussed. Such a study is expected to be helpful in furthering our understanding the effects of cooling treatments on the microstructure and oxidation resistance of the coatings.

Experimental Procedures

Coating Fabrication

The nickel-based high-temperature alloys DZ417G with nominal alloy composition (at.%) of Ni–5.2Al–9.0Cr–10.0Co–4.4Ti–3.0Mo–0.19C–0.7V was used as a substrate. Rectangular specimens with dimensions of $10.0 \times 6.0 \times 2.5$ mm^3 were first gritblasted from 80 to 2000 mesh, ultrasonically cleaned and then electroplated with 12 μm of Pt. The specimens were sealed in the quartz tube in a vacuum of 10^{-2} Pa followed by a diffusion treatment for 2 h at 1000, 1100 and 1150 °C. After that, the specimens in the quartz tube cooled to room temperature to get furnace-cooled coatings. The water-quenched coatings were prepared by cooling the specimens in the quartz tube in water. As shown in Table 1, the coatings of 12 μm Pt-plated specimens prepared by diffusion treatment at 1000, 1100 and 1150 °C followed by furnace-cooling and water-quenching were represented with sample #1 to #6, respectively.

Table 1 Furnace-cooled and water-quenched coatings prepared by diffusion treatment at different temperatures followed by cooling

Sample no.	Diffusion temperatures (°C)	Cooling treatment
#1	1000	Furnace-cool
#2	1100	Furnace-cool
#3	1150	Furnace-cool
#4	1000	Water-quench
#5	1100	Water-quench
#6	1150	Water-quench

Table 2 Pt-modified coatings prepared by pack cementation with varying Al contents in the pack

Coating no.	Pack composition (wt%)	Coating types and deposition temperature
#7	1Al + 2NH_4Cl + Al_2O_3 (Bal.)	Furnace-cooled coating, 900 °C
#8	4Al + 2NH_4Cl + Al_2O_3 (Bal.)	Furnace-cooled coating, 900 °C
#9	6Al + 2NH_4Cl + Al_2O_3 (Bal.)	Furnace-cooled coating, 900 °C
#10	1Al + 2NH_4Cl + Al_2O_3 (Bal.)	Water-quenched coating, 900 °C
#11	4Al + 2NH_4Cl + Al_2O_3 (Bal.)	Water-quenched coating, 900 °C
#12	6Al + 2NH_4Cl + Al_2O_3 (Bal.)	Water-quenched coating, 900 °C

After that, the specimens were deposited with Al by pack cementation process. In this study, the pack powder mixtures for deposition contain Al as deposition elements, NH_4Cl salt as an activator, and Al_2O_3 powder as an inert filler. At high temperatures, the halide salt will react with the deposition elements to form a series of halide vapor species including the deposition elements such as AlCl and $AlCl_2$. The coating is formed through the reduction of these species and the subsequent interdiffusion between the deposited elements and the substrate at the deposition temperature. In order to protect the sample from being oxidized, it is necessary to make the argon gas flow into the furnace. The composition series was xAl–2NH_4Cl-(98-x) Al_2O_3 (wt%) with varying Al content ($x = 1$, 4 and 6). The whole pack was heated to 800 °C for 2 h. The post heat-treatments were performed at 1000 °C in vacuum for 6 h to homogenize the microstructure of the coatings. The Al deposited coatings were prepared with samples #3 and #6 deposition of Al by pack cementation process. As shown in Table 2, the coatings prepared in different Al contents in the packs at 1, 4 and 6 wt%, were represented with coating #7 to #12, respectively.

Oxidation Resistance Tests and Characterization

Oxidation tests were carried out at 1000 °C in still air for different times in the range of 5–100 h using a muffle furnace. Mass gain of the coatings was measured by an analytical balance. The phase constitutions of the coatings were determined by the D/MAX-3C X-ray diffraction (XRD) using Cu $K_{\alpha 1}$ radiation ($\lambda = 0.1541$ nm) in the range $2\theta = 20$–100° with a step size of 0.02° and a counting time of 1 s per

step. The cross-sectional micrographs were acquired and the surface morphologies of the coatings were characterized by an S-3400N scanning electron microscope (SEM) equipped with energy-dispersive X-ray (EDX) spectroscopy.

Results

Microstructure of Diffusion Coating After Heat Treatment Followed by Furnace-Cooling and Water-Quenching Treatment

Figure 1 shows representative X-ray diffractograms (XRD) and cross-sectional SEM images of simple Pt-modified coatings at 1000 °C (sample #1), 1100 °C (sample #2), and 1150 °C (sample #3). As shown in Fig. 1a, the phase of samples #1, #2 and #3 is α-NiPt. According to Fig. 1b–d, the coating is made up of an outer layer and an interdiffusion zone (IZ) with two different phases. Similar phases are also found in the IZ due to the Pt effect [17]. The Al content is high in the black zone (Al-rich phase) and the gray zone is rich in Ni (Ni-rich phase).

XRD analysis and cross-sectional SEM images of water-quenched coatings at 1000 °C (sample #4), 1100 °C (sample #5) and 1150 °C (sample #6) are shown in Fig. 2. According to XRD in Fig. 2a, the phase of samples #4, #5 and #6 is γ′-

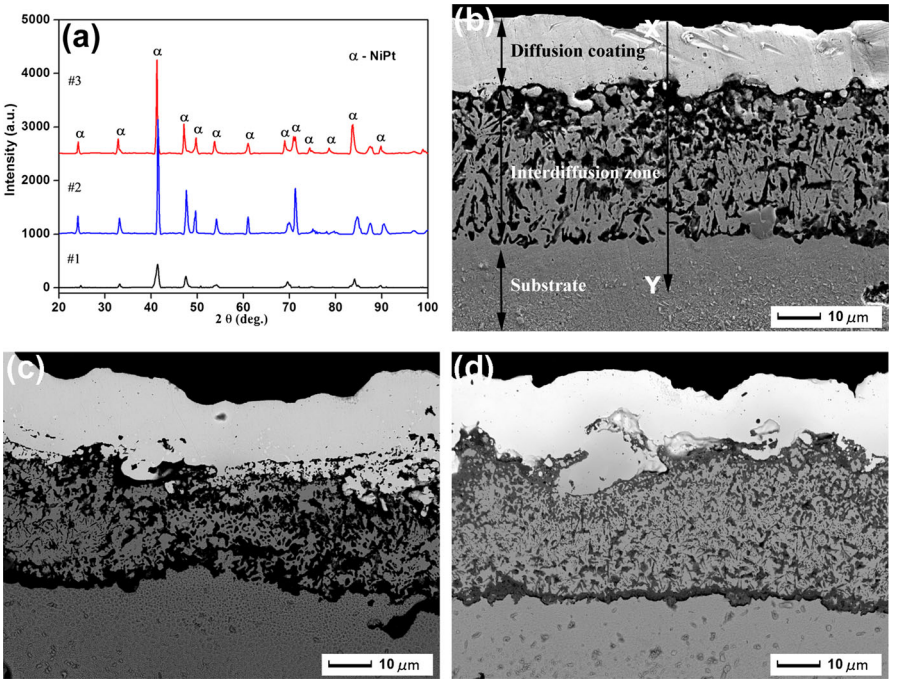

Fig. 1 X-ray diffractograms (**a**), SEM cross-sectional images of simple Pt-modified coatings **b** #1, **c** #2 and **d** #3 after furnace-cooling

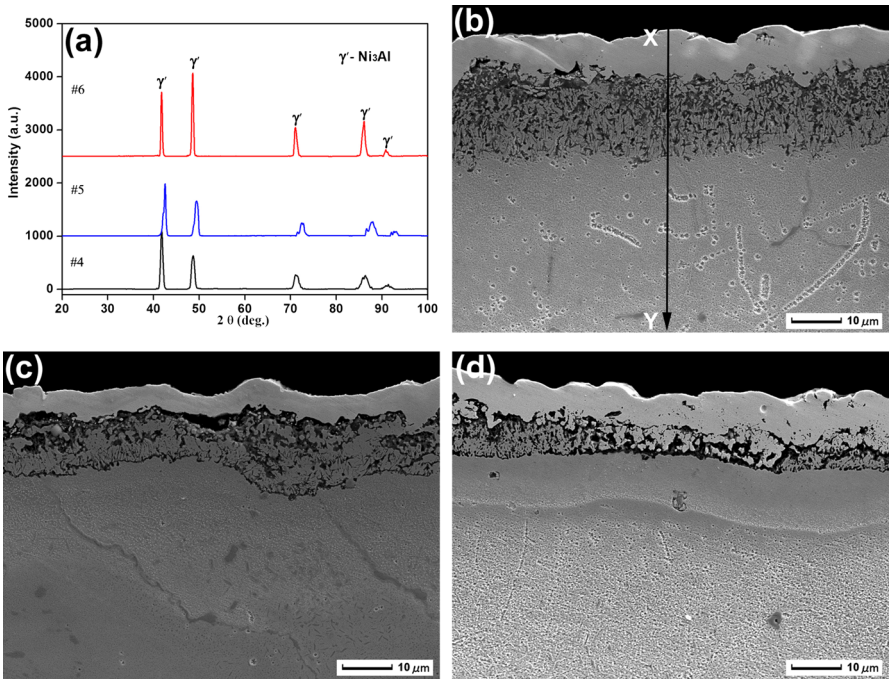

Fig. 2 X-ray diffractograms (**a**), SEM cross-sectional images of simple Pt-modified coatings **b** #4, **c** #5 and **d** #6 after water-quenching

Ni_3Al, which is different to the furnace-cooled coatings. The SEM results (Fig. 2b–d) show that the coatings have two layers including the outer layer and the IZ.

The Pt, Ni, Cr and Al concentration profiles from X to Y of samples #1 (Fig. 1b) and #4 (Fig. 2b) are compared in Fig. 3. The concentration profiles are divided into different zones in order to compare samples #1 and #4. Figure 3a shows the Pt line scan analysis results of samples #1 and #4. The curves are divided into zone-1-1, zone-1-2 and zone-1-3. According to the zone-1-1 and zone-1-2, Pt diffuses to the substrate and most of Pt is distributed in the coating. Pt is not found in the IZ and substrate of sample #1 while a few Pt exists in the IZ of sample #1 (see the zone-1-3). Figure 3b indicates that, in sample #1, Ni diffuses into the coating from the substrate and the Ni content of the coating (see the zone-2-1) is lower than in the IZ (see the zone-2-2) and the substrate (see the zone-2-3) because the height of the zone-2-1is lowest. However, in sample #4, Ni is uniformly distributed from coating to substrate (see the Ni curve of sample #4 in Fig. 3b). Figure 3c shows the Cr concentration profiles in samples #1 and #4. In sample #1, the curve of zone-3-1 and zone-3-2 is lower than zone-3-3 and zone-3-4, indicating that Cr out-diffuses into the IZ but does not further diffuse to the coating. However, in sample #4, there is equal Cr content in coating, IZ and substrate. The Al concentration profiles are shown in Fig. 3d. Compared the zone-4-1, zone-4-2 with zone-4-3 and zone-4-4 in the sample #1, it can be concluded that the Al content in the IZ and coating is higher

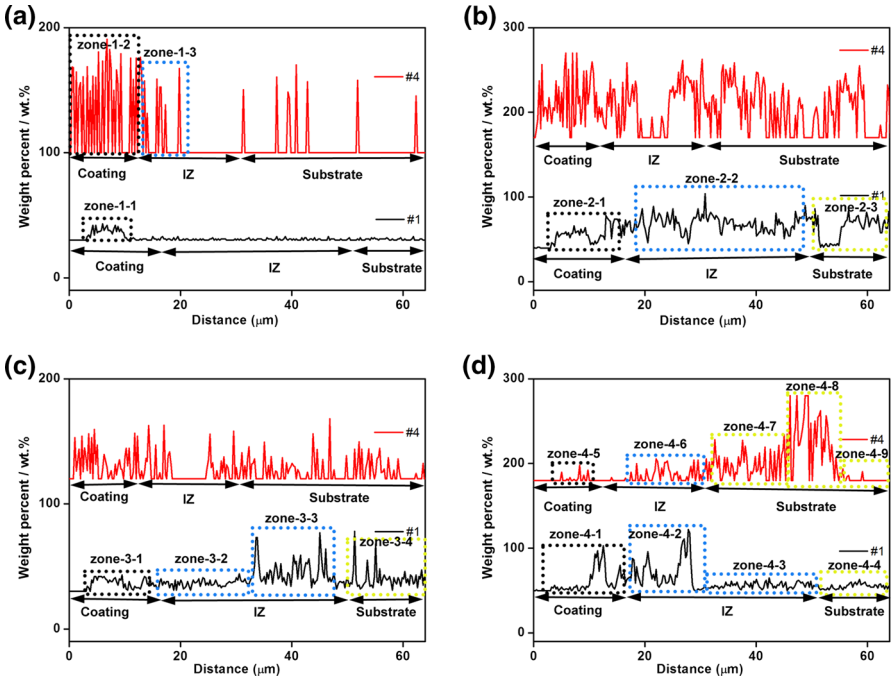

Fig. 3 Concentration profiles of different elements **a** Pt, **b** Ni, **c** Cr and **d** Al from X to Y in the coating #1 and #4

than the substrate. This is to say, Al tend to be rich in the coating in the α-NiPt. Yet, in sample #4, only few Al diffuse into the coating (see the zone-4-5) and IZ (see the zone-4-6). Most of Al exists in the substrate (see the zone-4-7 to zone-4-9), which indicates that it is difficult for Al to out-diffuse in the γ'-Ni_3Al.

Microstructure of Pt-Aluminide Coatings After Pack Cementation Process

Figure 4 shows the X-ray diffractograms and corresponding SEM cross-sectional images with sample #3 following deposition of Al in different amounts of 1 wt% (coating #7), 4 wt% (coating #8) and 6 wt% (coating #9). According to Fig. 4a, the phases of the coatings are ε-PtAl (coating #7) and ξ- $PtAl_2$ (coatings #8 and #9) respectively. Figure 4b–d indicates that the coatings exhibited a two-layer microstructure. There are also two phases in the IZ and the black phase is embedded in the gray phase.

Figure 5 presents the X-ray diffractograms and corresponding SEM cross-sectional images with sample #6 following deposition of Al in different amounts of 1 wt% (coating #10), 4 wt% (coating #11) and 6 wt% (coating #12). According to the X-ray diffractograms in Fig. 5a, the phases of the coatings are γ'-$(Ni, Pt)_3Al$ (coating #10) and ξ-$PtAl_2$ (coatings #11 and #12) after pack cementation.

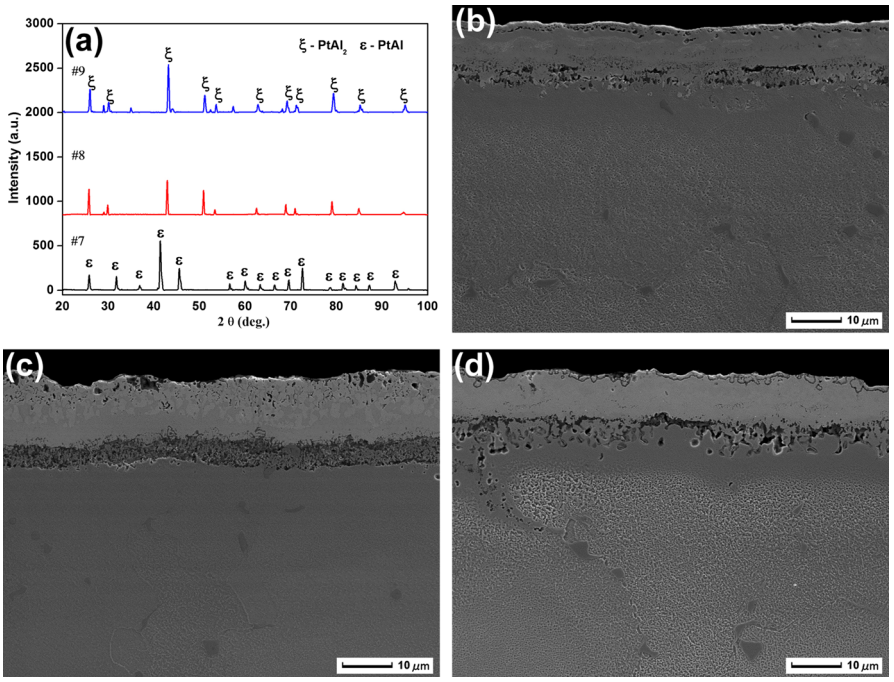

Fig. 4 X-ray diffractograms (**a**), SEM cross-sectional images of diffusion coatings **b** #7, **c** #8 and **d** #9 with sample #3 aluminizing by pack cementation process

Figure 5b–d shows that the coatings are made up of two layers including the out-layer and IZ. The smallest IZ is in coating #11.

Oxidation Resistance of Al Deposited Coatings at 1000 °C in Air

The oxidation kinetics of the furnace-cooled coatings after 100 h of oxidation is performed on Fig. 6a, with the oxidation of the coatings evolving in two stages. In the first, a sharp increase occurs due to the formation of the oxide layer. However, as the oxidation proceeds, the protective oxide gradually thickens such that the oxidation rate decreases and the curve becomes parabolic. The weight change for coating #9 is important. Coating #7 has the lowest weight gain, which means it exhibited the best oxidation resistance among all the coatings. Figure 6b presents the X-ray diffractograms of the coatings after oxidation. According to Fig. 6b, the phases of coatings #7 and #8 are $TiO_2 + Pt + Al_2O_3$ while coating 9# is transformed to $TiO_2 + Pt + Al_2O_3 + NiO$.

Figure 6c–h shows the surface morphologies and cross-sectional images of the coatings after oxidation. The microstructures of coatings #7 (Fig. 6c) and #8 (Fig. 6e) are mainly composed of three kinds of phases including the block TiO_2 (point +1), the granular Al_2O_3 (point +2) and the pin-striped Pt (point +3). The shell-shaped phase NiO is formed on the surface of coating #9 (Fig. 6g). According to the cross-sectional images in Fig. 6a, d, f, h continuous, dense Cr_2O_3 (point +4)

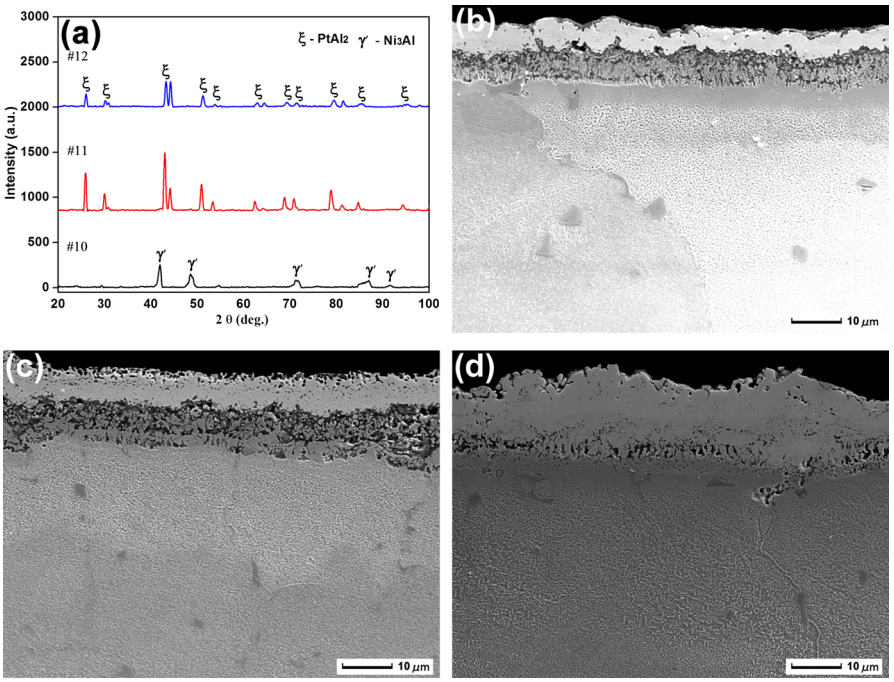

Fig. 5 X-ray diffractograms (**a**), SEM cross-sectional images of diffusion coatings **b** #10, **c** #11 and **d** #12 with sample #6 aluminizing by pack cementation process

and Al_2O_3 (point +5) was formed on the surface of the coatings. The EDS results (Fig. 6i) shows that, points +1 and +2 include O, Al, Ti, Cr and Ni. The ratios of Ti, Al and O are consistent with TiO_2 phase (point +1) and Al_2O_3 (point +2). It should be noted that point +3 is mainly made up of Pt, which is consistent with the XRD result in Fig. 6b. It was found that Cr-oxides such as Cr_2O_3 were not detectable from XRD but existed in the coating according to the EDS results of points +4 and +5.

Figure 7a shows the oxidation kinetics of the water-quenched coatings after 100 h of oxidation. The oxidation of the coatings evolves in similar stages to the furnace-cooled coatings. The weight change for coating #11 is important and coating #10 has the lowest weight gain. The XRD results in Fig. 7b indicate that $Cr_2NiO_4 + TiO_2 + Cr_2O_3$ (coating #10) and $TiO_2 + Cr_2O_3$ (coatings #11 and #12) are formed after oxidation.

The surface morphologies and SEM images of the coatings are shown in Fig. 7c–i after oxidation. The microstructure of coating #10 is made up of three different phases including the globular Cr_2NiO_4 (point +1), the granular Cr_2O_3 (point +2) and the nubby TiO_2 (point +3) in Fig. 7c. According to Fig. 7e, g, only two kinds of phases such as Cr_2O_3 and TiO_2 are produced above coatings #11 and #12. In addition, there is much more Cr_2O_3 on the surface of coatings #12 than coating #11. According to the cross-sectional images in Fig. 7d, f, h, a continuous, dense Cr_2O_3 was formed on the surface of the coatings. From the EDS results in Fig. 7f, it can be seen that points +1,

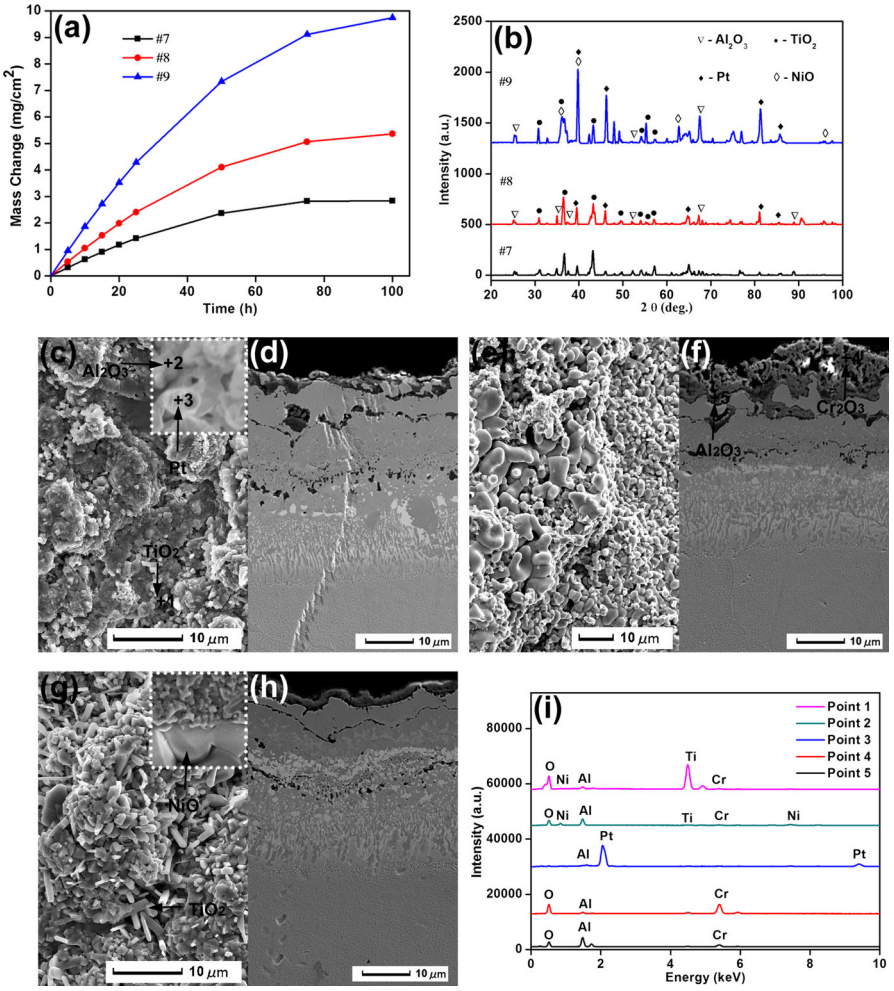

Fig. 6 Isothermal oxidation kinetics (**a**), X-ray diffractograms (**b**), SEM images (**c**), (**e**) and (**g**) of the surface morphologies and cross-sectional images of the coatings (**d**), (**f**) and (**h**) of the coatings #7, **d** #8 and **e** #9 and EDS results (**i**) after oxidation at 1000 °C in air

+2, and +3 include O, Al, Ti, Cr and Ni. The ratios of O, Ti, Cr and Ni are according with Cr_2NiO_4 (point +1), TiO_2 (point +2) and Cr_2O_3 (point +3).

Discussion

Mechanism Analyses of Phase Transformations in Different Cooling Rates and Their Effects on the Distribution of Cr in Coatings

According to the calculations, a strong tendency towards ordering was found in bulk $Ni_{1-x}Pt_x$ [18] and $(Ni_{1-x}Pt_x)_3Al$ alloys [19], which favors the formation of nearest-

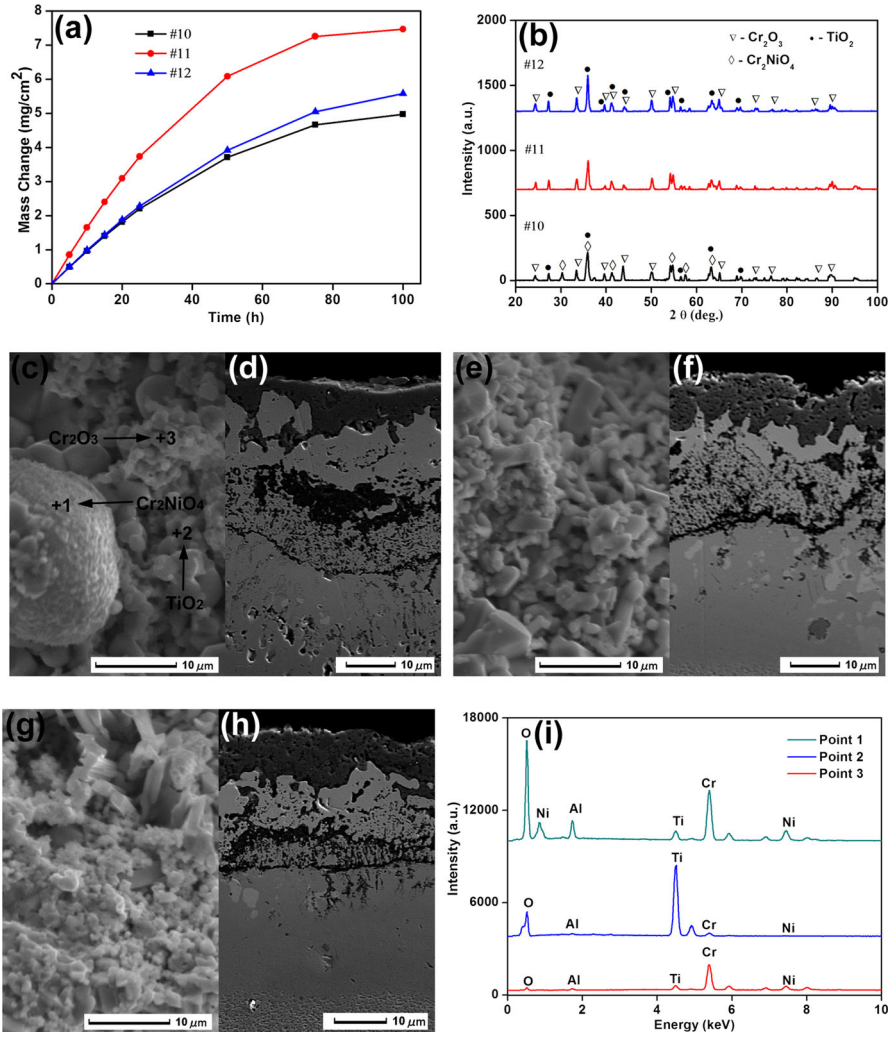

Fig. 7 Isothermal oxidation kinetics (**a**), X-ray diffractograms (**b**), SEM images (**c**), (**e**) and (**g**) of the surface morphologies and cross-sectional images of the coatings (**d**), (**f**) and (**h**) of the coatings #10, **d** #11 and **e** #12 and EDS results (**i**) after oxidation at 1000 °C in air

neighbor Ni-Pt bond. Due to strong Ni-Pt interactions, the segregation of Pt on Ni site may cause the formation of the α-NiPt phase. The strong tendency of Pt atoms to segregate for Ni atoms in γ′-(Ni, Pt)$_3$Al can have an obvious effect on its microstructure. The main point defects in Ni-rich L1$_2$ γ′-Ni$_3$Al are Ni antisites, which are confirmed by the experimental observations by Badura [17] and first-principles study by Fu [20]. Figure 8 shows the formation mechanisms of γ′-(Ni, Pt)$_3$Al and α-NiPt. In Fig. 8a, Pt diffuses into the cell and replaces Ni atom in the face-centered position at high temperature. After water quenching, there is not

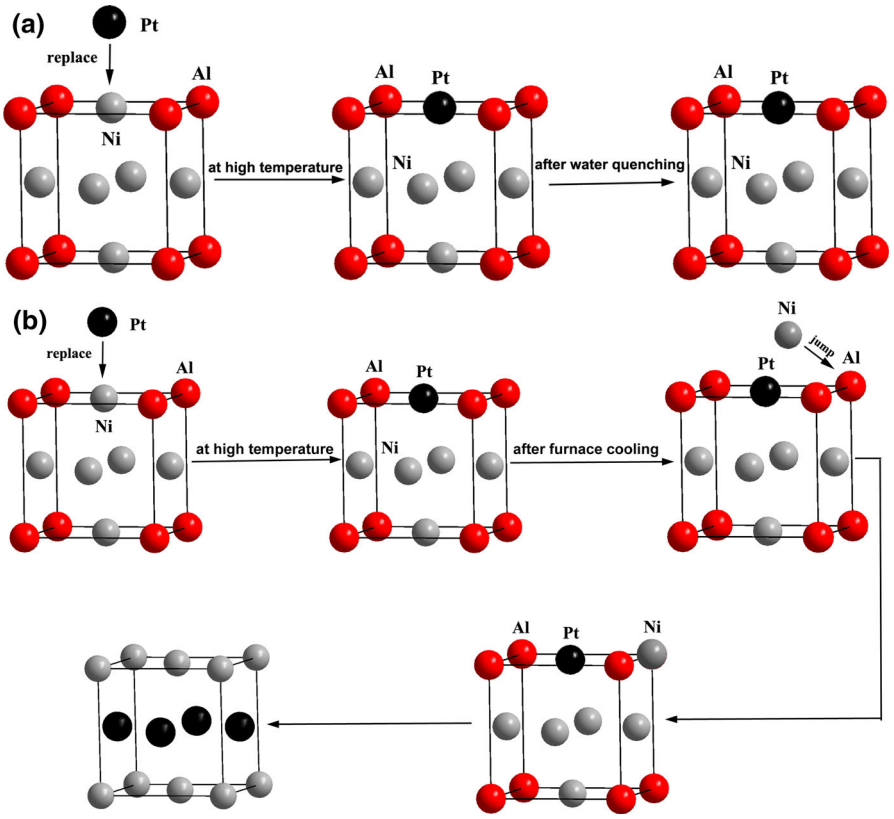

Fig. 8 The formation mechanisms of **a** γ'-(Ni, Pt)$_3$Al and **b** α-NiPt

enough time for Ni to jump into the Al site. As a result, the stable high-temperature phase γ'-(Ni, Pt)$_3$Al is kept at room temperature. According to Fig. 8b, the Ni atoms replaced by Pt may jump into an Al site and Ni antisites are formed in the cell during the furnace cooling process because of the slow cooling rate. When four Ni atoms in the face-centered positions are replaced by Pt atoms and jump into the vertex positions, the α-NiPt phase is formed. The Ni:Al atom ratio in the γ'-Ni_3Al is 3:1. This is to say, two Ni atoms will be remained after Ni jumps to the Al site. Similar to the step 3 in Fig. 8b, the remainder Ni atoms will be transformed to γ-Ni.

γ'-Ni_3Al has an ordered $L1_2$ (Cu_3Au-type) structure that consists of two sublattices, i.e., the a-sublattice (the face centers) and the b-sublattice (cube corner). In its perfectly ordered state at the stoichiometric composition, the a-sublattice is entirely occupied by Ni atoms and the b-sublattice is entirely occupied by Al atoms [12]. The results of the present investigation reveal that the microstructure of coatings is strongly affected by thermal treatments. The appearances of a Cr-rich γ'-Ni_3Al and Cr-depleted α-NiPt predict the microstructure change induced by fast cooling rate. According to Fig. 3c, the distribution of Cr in the coatings was affected by the cooling rate. In fact, this is caused by the phase transformations at fast

cooling rate because Cr tended to dissolve in the γ′-Ni_3Al matrix during heat treatment [21]. Perez et al. also pointed out that high cooling rates generated a non-equilibrium microstructure consisting of γ′-Ni_3Al and Cr-rich phase which tended to dissolve in the γ′-Ni_3Al matrix after annealing at high temperatures [21]. The preferential segregation of Cr to the γ′-Ni_3Al has been confirmed by the HAADF-STEM image [22]. Ochiai et al. [23] pointed out that γ′-Ni_3Al could accommodate a certain number of Cr atom. Lu et al. [24] suggested that Cr atoms mainly occupied b-sublattice and only very few Cr atoms occupied a-sublattice. This is to say, Cr tend to dissolve into γ′-Ni_3Al, forming complex $Ni_3(Al_{1-x}Cr_x)$ phase. Jiang et al. [25] and Chaudhari et al. [26] also found that Cr atoms preferred to occupy b-sublattice in $L1_2$ γ′-Ni_3Al by using first-principle. Figure 8a, b show that the coating is γ′-$(Ni, Pt)_3Al$ at high temperatures. As a result, Cr atoms dissolve into the γ′-$(Ni, Pt)_3Al$ coating. However, γ′-$(Ni, Pt)_3Al$ was transformed to α-NiPt after furnace-cooling treatment. The dissolved Cr atoms in α-NiPt may be released and diffuse into IZ or substrate according to Fig. 3c.

The Effects of Phase Transformations on the Oxidation Resistance of Coatings

During the pack cementation process, Al powders react with NH_4Cl salts to form gaseous Al-chloride species AlCl at high temperatures. AlCl diffuses to the surface of the substrate (Cr-rich γ′-$(Ni, Pt)_3Al$ and Cr-depleted α-NiPt) and release the active Al atoms (represented by [Al]). Cr-rich γ′-$(Ni, Pt)_3Al$ coatings would be transformed to γ′-Ni_3Al or ξ-$PtAl_2$ while Cr-depleted α-NiPt coatings are transformed to ε-PtAl or ξ-$PtAl_2$. When comparing with the line scan analysis results of coatings #3 and #6 in Fig. 3, it is obvious that more Cr out-diffuse into the IZ in water-quenched coatings than in furnace-cooled coatings (see Fig. 3c). In addition, the case of Al distribution in water-quenched coatings and furnace-cooled coatings is opposite to that of Al (see Fig. 3d). It has been reported that Cr has a positive chemical interaction with Al in the Ni–Al–Cr system [27]. Therefore, Cr addition to Ni–Al alloys has the effect of increasing the chemical activity of Al. This positive Cr effect would cause a steeper Al activity gradient in the coating. It was reported that the Al interdiffusion flux in the Ni–Pt–Al alloy side of a diffusion couple with the Ni–Al–Cr alloy was smaller than in a couple with Ni–Al [28], which also indicates that Cr has the effect of increasing the chemical activity of Al. As a result, the addition of Cr can affect the diffusion and distribution of Al in the coatings because Cr is accommodated in the $L1_2$ γ′-Ni_3Al and the Al concentration was reduced [23, 26]. Especially, the addition of Cr also can enhance the high-temperature resistance of γ′-Ni_3Al [29, 30].

Investigations on a variety of alloy coatings have shown that the coating microstructure has a significant influence on the oxidation behavior of coatings because the rapid diffusion can promote the selective oxidation behavior [31]. Indeed, the oxidation formations of furnace-cooled and water-quenched coatings are different, which is caused by the distribution and diffusion of Cr and Al. when compared with water-quenched coatings, the furnace-cooled coatings revealed a slower oxidation rate and showed better oxidation resistance, which might be

originated from the effect of Cr. The oxidation resistance of coatings is determined by the surface oxide layers and their compactness and integrity [32]. Al_2O_3 is a most desired protective oxide layer for superalloys in high-temperature because its high density can prevent the diffusion of O_2. The integrity of an outer Al_2O_3 is required to form a protective oxide [33]. The furnace-cooled coatings tend to form Al_2O_3 although a little of Cr_2O_3 was found according to the EDS result after oxidation. Lee et al. has reported that Cr would exist in the oxide scale as dissolved ions, so the Cr-oxides were not detectable from XRD [34]. The water-quenched coatings are transformed to Cr_2O_3 after oxidation. The formation of Al_2O_3 in coatings is a key factor to form an integrated outer protective oxide to improve the oxidation resistance. It has been also reported that the addition of Cr in coatings can increases the oxidation resistance by the formation of protective chromium oxide films on the free surface [35]. The reason why the oxide formation differs with Cr-rich and Cr-depleted coatings may be due to the ternary element effect of Cr in Ni–Al. It has been reported that the addition of Cr to Ni–Al bulk alloy can obviously enhance the protection, and reduce the Al quantity demanded in Ni–Al alloy to form Al_2O_3 which acts a continuous protective oxide layer in oxidizing and corrosive environments [32, 36]. Based upon the above the oxidation tests, the Cr effect on the oxidation resistance of coatings can be attributed to the content of Cr in coatings. For the Cr-rich coatings, the enrichment of Cr prevents Al from diffusing into the coatings and the Al concentration is reduced [34]. As a result, Cr would react with O_2 to form Cr_2O_3 after oxidation. Nevertheless, the Cr-depleted coatings are transformed to Al_2O_3 because a moderate amount of Cr added in the coatings can reduce the amount of Al required to form Al_2O_3 [32, 36] and promote the formation of a continuous outer Al_2O_3 layer during the oxidation test [33]. All the processes are described in Fig. 9. According to Fig. 9a, in the operating environment of turbine, oxygen diffuses on the surface of coating, and then the furnace-cooled coatings including ε-PtAl and ξ- $PtAl_2$ react with O_2 to form Al_2O_3. Furthermore, reactive Pt atoms (represented by [Pt]) are released. [Pt] in-diffuses into the coating and promotes the diffusion of the active Al atoms (represented by [Al]). During this process, Pt on the surface of the coatings will drop significantly due to interdiffusion [37]. A further contributing factor is that the Pt-containing γ' exhibits subsurface Pt enrichment during the very early stages of oxidation, which would reduce Ni availability and increase the Al supply to the evolving scale, thus kinetically favoring Al_2O_3 formation [38]. Indeed, the addition of Pt is beneficial in kinetically establishing a protective and continuous Al_2O_3 scale [39]. In addition, the active Ti atoms (represented by [Ti]) may also out-diffuse and react with O_2. Figure 9b shows the oxidation formation of water-quenched coatings including ε-PtAl and ξ- $PtAl_2$, which is different from that of furnace-cooled coatings. Because of higher Cr in the water-quenched coatings than furnace-cooled coatings (see Fig. 6c), the diffusion of Al is promoted. As a result, most of Al would in-diffuses and the active Cr atoms (represented by [Cr]) react with O_2 to form Cr_2O_3. The oxidation mechanism of water-quenched coating γ'-$(Ni, Pt)_3Al$ is shown in Fig. 9c. At the beginning of the process, γ'-$(Ni, Pt)_3Al$ reacts with O_2 and NiO is formed. After that, the released [Al], [Ti] and [Cr] diffuse into the coating. [Cr] is rich in the coating and can promote the diffusion of [Al]. As a result, only a little of Al_2O_3 was formed in the

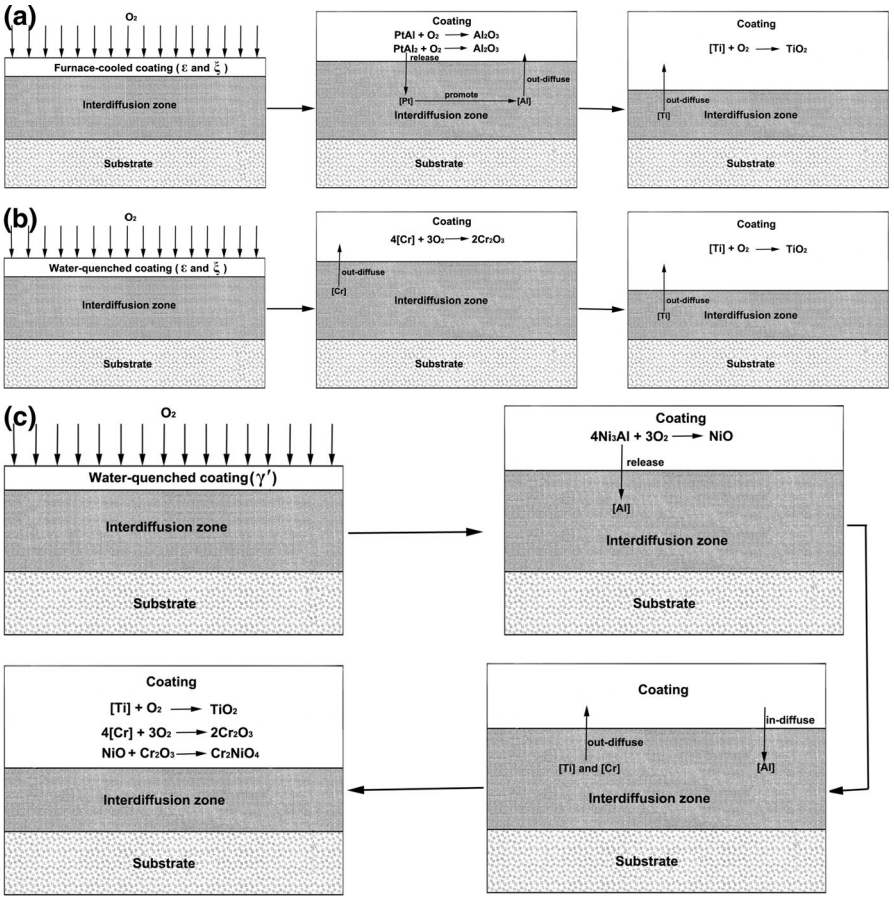

Fig. 9 The schematic diagram in the formation process of oxidation tests **a** ε-PtAl coating, **b** ξ-$PtAl_2$ coating and γ′-(Ni, $Pt)_3Al$ coating

coating. In the next process, [Ti] and [Cr] react with O_2 to form TiO_2 and Cr_2O_3. Because of the strong reaction between NiO and Cr_2O_3, the Cr_2NiO_4 is formed at the end of the process.

Conclusions

Pt-Aluminide coatings were prepared by diffusion treatments at high temperatures followed by furnace-cooling and water-quenching treatments. The phase of furnace-cooled coatings was α-NiPt while that of water-quenched coatings was γ′-(Ni, $Pt)_3Al$. After pack cementation, α-NiPt coating was transformed to ε-PtAl or ξ-$PtAl_2$ while γ′-(Ni, $Pt)_3Al$ coating was transformed to γ′-Ni_3Al or ξ-$PtAl_2$. Fast cooling rate has an obvious effect on the diffusion behavior and distribution of the

elements especially Cr. The level of Cr in the coatings has profound influences on the formation of protective oxide layers. The enrichment of Cr in the water-quenched coatings causes the formation of different oxidation states compared to the furnace-cooled coatings. The water-quenched coatings tend to form Cr_2O_3, whereas the formation of Al_2O_3 occurs in the furnace-cooled coatings after the oxidation.

Acknowledgments This work was supported by the National Natural Science Foundation of China (NSFC) under Grant 51271107, the Shanghai Committee of Science and technology, China under Grant Nos. 10JC1405100 and 11520701200, and the Innovation Program of Shanghai Municipal Education Commission under Grant No. 13ZZ077.

References

1. K. A. Marino and E. A. Carter, *Acta Materialia* **58**, 2726 (2010).
2. C. Leyens, I. G. Wright and B. A. Pint, *Oxidation of Metals* **54**, 401 (2000).
3. K. Y. Kim, S. Shin, D. H. Lee and H. H. Cho, *International Journal of Heat Mass and Transfer* **54**, 5192 (2011).
4. B. Gleeson, *Journal of Propulsion Power* **22**, 375 (2006).
5. A. V. Put, D. Oquab, E. Pere, A. Raffaitin and D. Monceau, *Oxidation of Metals* **75**, 247 (2011).
6. N. P. Padture, M. Gell and E. H. Jordan, *Science* **296**, 280 (2002).
7. I. Spitsberg and K. More, *Materials Science and Engineering A* **417**, 322 (2006).
8. J. A. Haynes, B. A. Pint, K. L. More, Y. Zhang and I. G. Wright, *Oxidation of Metals* **58**, 513 (2002).
9. D. R. Mumm, A. G. Evans and I. T. Spitsberg, *Acta Materialia* **49**, 2329 (2001).
10. B. Gleeson, W. Wang, S. Hayashi and D. Sordelet, *Materials Science Forum* **461–464**, 213 (2004).
11. B. Gleeson, B. Li, D. Sordelet and W.J. Brindley, US Patent No. 2006127695 (2006).
12. C. Jiang and B. Gleeson, *Acta Materialia* **55**, 1641 (2007).
13. T. Izumi, N. Mu, L. Zhang and B. Gleeson, *Surface and Coatings Technology* **202**, 628 (2007).
14. S. Sundaram, C. A. Johnson, D. M. Lipkin and J. W. Hutchinson, *Journal of Applied Mechanics* **80**, 001002 (2013).
15. R. W. Jackson and M. R. Begley, *International Journal of Solids and Structures* **51**, 1364 (2014).
16. V. K. Tolpygo, J. R. Dryden and D. R. Clarke, *Acta Materialia* **46**, 927 (1998).
17. K. Baduragergen and H. E. Schaefer, *Physical Review B* **56**, 3032 (1997).
18. C. E. Dahmnai, M. C. Cadeville, J. M. Sanchez and J. I. Moranlopez, *Physical Review Letters* **55**, 1208 (1985).
19. C. Jiang, D. J. Sordelet and B. Gleeson, *Physical Review B* **72**, 184203 (2005).
20. C. L. Fu and G. S. Painter, *Acta Materialia* **45**, 481 (1997).
21. P. Perez, P. Gonzalez, G. Garces, G. Caruana and P. Adeva, *Journal of Alloys and Compounds* **302**, 137 (2000).
22. S. V. Raju, A. A. Oni, B. K. Godwai, J. Yan, V. Drozd, S. Srinivasan, J. M. LeBeau, K. Rajan and S. K. Saxena, *Journal of Alloys and Compounds* **619**, 616 (2015).
23. S. Ochiai, Y. Oya and T. Suzuki, *Acta Metallurgical* **32**, 289 (1984).
24. Y. L. Lu, D. W. Jia, T. T. Hu, Z. Chen and L. C. Zhang, *Superlattices and Microstructures* **66**, 105 (2014).
25. C. Jiang, D. J. Sordelet and B. Gleeson, *Acta Materialia* **54**, 1147 (2006).
26. M. Chaudhari, J. Tiley, R. Banerjee and J. Du, *Materials Science and Engineering A* **21**, 055006 (2013).
27. J. A. Nesbitt and R. W. Heckel, *Metallurgical and Materials Transactions A* **18**, 2075 (1987).
28. S. Hayashi, W. Wang, D. J. Sordelet and B. Gleeson, *Metallurgical and Materials Transactions A* **36**, 1769 (2005).
29. Z. Y. Liu and W. Gao, *Oxidation of Metals* **55**, 481 (2001).
30. S. C. Choi, H. J. Cho and D. B. Lee, *Oxidation of Metals* **46**, 109 (1999).
31. Z. Y. Liu and W. Gao, *Oxidation of Metals* **55**, 481 (2001).
32. Y. Y. Xing, B. Dai, X. H. Wei, Y. J. Ma and M. Wang, *Vacuum* **107**, 101 (2014).

33. I. A. Kvernes and P. Kofstad, *Metallurgical and Materials Transactions B* **3**, 1511 (1972).
34. D. B. Lee and M. L. Santella, *Materials Science and Engineering A* **374**, 217 (2004).
35. C. T. Liu and V. K. Sikka, *Journal of Metals* **38**, 19 (1986).
36. S. W. Guan and W. W. Smeltzer, *Oxidation of Metals* **42**, 375 (1994).
37. J.A. Haynes, B.A. Pint, Y. Zhang and I.G. Wright, *Surface and Coatings Technology* **203**, 413 (2008).
38. S. Hayashi, T. Natira and B. Gleeson, *Materials Science Forum* **522–523**, 229 (2005).
39. V. Deodeshmukh and B. Gleeson, *Surface and Coatings Technology* **202**, 643 (2007).